Journal of Volcanology and Geothermal Research 447 (2024) 108031

Contents lists available at ScienceDirect

Journal of Volcanology and Geothermal Research

journal homepage: www.journals.elsevier.com/journal-of-volcanology-and-geothermal-research

# PROMETHEUS: Probability in the Mediterranean of Tephra dispersal for various grain sizes. A tool for the evaluation of the completeness of the volcanic record in medial-distal archives

E. Billotta [a,*], R. Sulpizio [a], J. Selva [b], A. Costa [c], M. Bebbington [d]

[a] Dipartimento di Scienze della Terra e Geoambientali, Università di Bari, Bari, Italy
[b] Dipartimento di Scienze della Terra, dell'Ambiente e delle Risorse, Università degli Studi di Napoli "Federico II", Napoli, Italy
[c] Istituto Nazionale di Geofisica e Vulcanologia (INGV), Sezione di Bologna, Bologna, Italy
[d] Institute of Fundamental Sciences - Statistics, Massey University, Palmerston North, New Zealand

ARTICLE INFO

*Keywords:*
Maps
Probability
Tephrostratigraphy
Catalogs
Statistics

ABSTRACT

PROMETHEUS is a statistical tool that allows creating maps showing the probability of finding tephra deposits of different grain sizes, originating from eruptions of a specific volcanic source, at any location around the vent. It couples wind profiles at different heights in the Mediterranean area with terminal velocity of volcanic particles. The input parameters include the height of the eruption column (which characterizes the intensity of the eruption), wind statistics (directions and intensities), and tephra deposits of a selected grain size. In particular, we used the parameterizations provided by Costa et al. (2016) and performed simulations using the HAZMAP tephra dispersal model to determine the maximum reachable distances that tephra can cover under weak, medium, and strong wind conditions (e.g. 7, 30, and 70 m/s velocities at the tropopause) and with column heights of 10, 20, and 30 km, depositing of at least the loading corresponding to 0.1 mm (corresponding to cryptotephra). Three alternative configurations of the model are validated analyzing first the eruptive source of Somma Vesuvius, with the related explosive eruptions from 22 ka Pomici di Base to the 1944 eruption. A further validation is made by comparing the probabilistic maps with the tephrostratigraphy of known marine and terrestrial cores using standard test of proportions (binomial distributions) and the binary logistic regression model, statistically quantifying the effectiveness of the model against the tephrostratigraphy recorded within this time frame. Based on this validation, a preferred configuration of PROMETHEUS is selected. PROMETHEUS probability maps will guide the selection of sampling sites for specific tephra deposits and could also support the study of the completeness of overall eruption catalogs over time.

## 1. Introduction

Assessing and predicting dispersal of ash from volcanic eruptions represent a very difficult task in volcanology (Sparks and Aspinall, 2004; Pfeiffer et al., 2005; Rose and Durant, 2009). This is due to the long residence time of ash in the atmosphere (Dellino et al., 2005; Sulpizio et al., 2008; Rose and Durant, 2009), the multiple processes that can affect it deposition (Armienti et al., 1988; Macedonio et al., 2005; Folch, 2012) and the ephemeral thickness they usually deposit over the landscape and marine realm (e.g. Wulf et al., 2004; Di Roberto et al., 2008; Lowe, 2011; Leicher et al., 2016; Insinga et al., 2019). These phenomena may result in patchy recognition of ash deposits in distal, and largely impact on tephrostratigraphy and its correlative potential among different sedimentary archives. They may also affect the inversion of data for modelling ash dispersal and probabilistic hazard assessment of ash deposition (e.g., Costa et al., 2006; Folch, 2012). For these reasons, the completeness of the tephrostratigraphic catalogs containing ash deposits is a key factor for the reliable assessment of tephra dispersal areas, which is the base for any volcanological and/or hazard assessment study. Even if many databases of volcanic activity like the Global Volcanism Program (Cottrell et al., 2010; Crosweller et al., 2012) exist, only few studies about incompleteness of volcanic records are available (Mead et al., 2014; Wang et al., 2020), and there are still not satisfactory techniques to estimate the degree of completeness of stratigraphic records in distal areas, which may significantly contribute to catalogs especially for large and old eruptions. In fact, numerous modern

* Corresponding author at: Dipartimento di Scienze della Terra e Geoambientali, Università di Bari, Bari, Italy
*E-mail addresses:* eli-billy@live.it, elisabetta.billotta7@gmail.com (E. Billotta).

https://doi.org/10.1016/j.jvolgeores.2024.108031
Received 29 September 2023; Received in revised form 21 January 2024; Accepted 14 February 2024
Available online 18 February 2024

volcanological studies concerning eruptions already previously studied underline how the eruptive history of the different volcanic districts is not yet well known, but instead requires considerable study and new statistical and probabilistic methodologies (Bebbington, 2020). Indeed, this would allow the use of the information recorded in locations where, for geological reasons, a well preserved long tephrostratigraphic record is available. Such locations are few, and in most of cases they are far from volcanoes, and potentially impacted in the far field by multiple volcanic sources (Wagner et al., 2008, 2019; Leicher et al., 2016, 2021). This is especially urgent in regions affected by ash deposition from many different volcanoes, such as the central Mediterranean area. Since the Pleistocene, the central Mediterranean region witnessed numerous volcanic eruptions sourced mainly from southern Italy volcanoes (Keller et al., 1978; Paterne et al., 1988; Wulf et al., 2004; Sulpizio et al., 2010). The recognition of the different tephra layers has allowed reconstruction of frequency maps, which are useful for improving the assessment of volcanic hazard (Sulpizio et al., 2014). However, the preservation of tephra in the middle and distal archives downwind of southern Italy volcanoes is sometimes largely incomplete, due to both discontinuous deposition and erosion. In order to reduce the uncertainty on dispersal area of ash, we need to consider a probabilistic approach that combines the characteristics of the eruption and the intensity of winds in both the stratosphere and troposphere.

Here we present an innovative probabilistic method that, by combining statistics of wind profiles over the last 30 years in southern Italy and inferred eruption intensity, allows us to calculate the probability for a given grain size to reach a given point downwind of the source volcano. The method is sufficiently simple to allow a rapid application to multiple volcanoes and volcanic areas, allowing the potential exploration of multiple sources without the need of large computational resources. We initially apply the method to Somma Vesuvius, which accounts for most of ash dispersal during late Pleistocene and Holocene in central Mediterranean area (Paterne et al., 1988; Sulpizio et al., 2010, 2014; Caron et al., 2012; Crocitti et al., 2018), then we demonstrate that the method is equally applicable to any other volcano of the area, provided that the validity of the meteorological conditions is approximately preserved.

The results were tested through a series of validation exercises, such as the comparison of the maps with the previously published geological data (Wulf et al., 2004; Di Roberto et al., 2008; Leicher et al., 2016; Insinga et al., 2019), tests of proportions via the binomial distribution (Bebbington et al., 2013; Selva et al., 2013; Grezio et al., 2017) and binary logistic regression model (logit) (Kereszturi et al., 2017; Ang et al., 2020).

The scripts used to produce the probability maps are available at: https://gitlab.com/bari_maps/probability_maps.git.

### 1.1. Volcanological and tephrostratigraphic framework

Somma Vesuvius is a stratovolcano characterized by an older edifice (Mount Somma) dissected by a summit caldera. The Vesuvius cone grew within the summit caldera after 79 CE (Cioni et al., 2000). In the last 22 ky the explosive activity of Somma Vesuvius witnessed the Plinian eruptions of the "Pomici di Base" (22,030 ± 175 cal yr BP; Bertagnini et al., 1998), Mercato (8890 ± 90 BP; Santacroce et al., 2008; Mele et al., 2011), Avellino (4365 ± 40 BP; Andronico et al., 1995; Santacroce et al., 2008) and Pompei (79 CE Sigurdsson et al., 1982) (Table 1). Sub-Plinian eruptions occurred at 19265 ± 105 cal yr BP (Pomici Verdoline; Andronico et al., 1995; Cioni et al., 2004, Santacroce et al., 2008), in the period between Avellino and 79 CE eruptions (named APs; Andronico and Cioni, 2002), in 472 CE (Pollena; Sulpizio et al., 2005) and 1631 CE (Rosi and Santacroce, 1983). After the 79 CE Plinian eruption the Somma Vesuvius activity alternated periods of closed and open conduit, with explosive eruptions occurred sporadically (Cioni et al., 2008).

The most recent period (1631–1944 CE) was characterized by open conduit conditions and persistent effusive, explosive or mixed activity, with a maximum of 7 year period of quiescence (Santacroce, 1987). Major, mixed effusive explosive eruptions occurred in 1822 CE, 1906 CE and 1944 CE (Arrighi et al., 2001), which is also the last eruption of Somma Vesuvius (Cole and Scarpati et al., 2010).

Initially, the reference targets used in this work are the core drilling of Lago di Monticchio (Table 2; Italy - 40.9 N, 15.6 E) and Lake Ohrid (Table 3; Republic of North Macedonia - 41.04 N, 20.71 E). Tables 2 and 3 contain information regarding the recognized tephra layers in Lake

**Table 1**
eruptions of Somma Vesuvius considered in this work from 22 Ka to 1944.

| Eruption | Age (a) | | | Column Height (b) | ML tephras | OL tephras | References |
|---|---|---|---|---|---|---|---|
| 1944 | 1944 | | CE | 10 | | | Arrighi et al., 2001 (a)(b) |
| 1906 | 1906 | | CE | 15 | | | Arrighi et al., 2001 (a)(b) |
| 1822 | 1822 | | CE | 5–10 | | | Arrighi et al., 2001 (a)(b) |
| 1794 | 1794 | | CE | 2 | | | Arrighi et al., 2001 (a)(b) |
| 1779 | 1779 | | CE | 3 | | | Arrighi et al., 2001 (a)(b) |
| 1730 | 1730 | | CE | 6 | | | Arrighi et al., 2001 (a)(b) |
| 1723 | 1723 | | CE | 2.8 | | | Arrighi et al., 2001 (a)(b) |
| 1707 | 1707 | | CE | 2.1 | | | Arrighi et al., 2001 (a)(b) |
| 1682 | 1682 | | CE | 2.2 | | | Arrighi et al., 2001 (a)(b) |
| 1631 | 1631 | | CE | 20 | X | | Santacroce et al.,2008 (a)(b) |
| AS5 | 540 | ± 30 | cal yr BP | 8 | | | Selva et al., 2022 (a)(b) |
| AS4 | 1100 | ± 70 | cal yr BP | 4 | | | Selva et al., 2022 (a)(b) |
| AS3 | 1310 | ± 30 | cal yr BP | 8 | | | Selva et al., 2022 (a)(b) |
| AS2 | 1470 | ± 60 | cal yr BP | 8 | | | Cioni et al., 2008 (a); Sulpizio et al., 2005 (b) |
| 512 d.C. | 512 | | CE | 15 | X | X | Cioni et al., 2011 (a)(b) |
| Pollena | 472 | | CE | 20 | X | X | Sulpizio et al., 2005 (a)(b) |
| S.Maria cycle | 305 | | CE | 10 | | | Cioni et al., 2008 (a)(b) |
| S.Maria cycle | 222–235 | | CE | 10 | | | Cioni et al., 2008 (a)(b) |
| S.Maria cycle | 203 | | CE | 10 | | | Cioni et al., 2008 (a)(b) |
| S.Maria cycle | 172 | | CE | 10 | | | Cioni et al., 2008 (a)(b) |
| Pomici di Pompei | 79 | | CE | 35 | X | | Sigurdsson et al., 1982 (a); Cioni et al., 2008 (b) |
| AP3 | 2710 | ± 60 | BP | 15 | X | | Cioni et al., 2008 (a); Andronico et al., 2002 (b) |
| AP2 | 3000 | ± 200 | BP | 15 | X | | Cioni et al., 2008 (a); Andronico et al., 2002 (b) |
| AP1 | 3220 | ± 65 | BP | 15 | | | Cioni et al., 2008 (a)(b) |
| Pomici di Avellino | 4365 | ± 40 | BP | 35 | X | | Andronico et al., 1995 (a); Santacroce et al., 2008 (b) |
| Pomici di Mercato | 8890 | ± 90 | BP | 22 | X | X | Santacroce et al., 2008 (a); Mele et al., 2011 (b) |
| Pomici Verdoline | 19,265 | ± 105 | cal yr BP | 20 | X | | Andronico et al., 1995 (a); Santacroce et al., 2008 (b) |
| Pomici di Base | 22,030 | ± 175 | cal yr BP | 25 | X | | Bertagnini et al., 1998 (a)(b) |

**Table 2**
core of the Lago di Monticchio. References: a) Wulf et al., 2004; b) Wulf et al., 2008; c) Wulf et al., 2012; d) Narcisi, 1996.

| Tephras | Age (yr BP) | | Age varve (yr BP)- 5% error | | Volcanic district | Eruption | References |
|---|---|---|---|---|---|---|---|
| | Data | (±) | Data | (±) | | | |
| TM-1* | 1631 | | 90 | 5 | Somma Vesuvius | 1631 | b |
| L1 | 79 | | | | Somma Vesuvius | Pomici di Pompei | d |
| TM-2b | 472 | | 1440 | 70 | Somma Vesuvius | Pollena | a |
| TM-2a | 512 | | 1420 | 1420 | Somma Vesuvius | 512 | a |
| TM-3b | 2710 | 60 | 4020 | 4020 | Somma Vesuvius | AP3 | a |
| TM-2-1 | 2920 | 160 | 3040 | 150 | Phlegrean volcanic district | Ischia-Cannavale o Chiarito | b |
| TM-2-2 | | | 3940 | 200 | Somma Vesuvius | AP5 | b |
| TM-3a* | | | 3990 | 200 | Somma Vesuvius | AP4 | b |
| TM-3c* | 3160 | 230 | 4150 | 210 | Somma Vesuvius | AP2 | b |
| TM-4* | 3590 | 25 | 4310 | 220 | Somma Vesuvius | Pomici di Avellino | b |
| TM-5b* | 4220 | 70 | 4660 | 230 | Phlegrean volcanic district | Astroni 1–3 | b |
| TM-5c* | 4620 | 40 | 5390 | 270 | Phlegrean volcanic district | Agnano Monte Spina | b |
| TM-5d* | 5150 | 30 | 5680 | 280 | Phlegrean volcanic district | Averno 1 | b |
| TM-5-2 | 5500 | 4500 | 7150 | 360 | Phlegrean volcanic district | Ischia | b |
| TM-6a* | 8010 | 35 | 9620 | 480 | Somma Vesuvius | Pomici di Mercato_final | b |
| TM-5-1 | 8500 | | 6590 | 330 | Phlegrean volcanic district | Ischia-Puzzillo | b |
| TM-6b* | | | 9680 | 480 | Somma Vesuvius | Pomici di Mercato_base | b |
| TM-6-1a | 8890 | 30 | 9890 | 490 | Phlegrean volcanic district | Campi Flegrei-Fondi di Baia | b |
| TM-7b* | 10,430 | 90 | 12,180 | 610 | Phlegrean volcanic district | CF-Pomici Principali | b |
| TM-6-4a | 11,010 | 60 | 11,670 | 580 | Phlegrean volcanic district | Campi Flegrei-Soccavo 5 | b |
| TM-6-4b | 12,140 | 100 | 11,890 | 590 | Phlegrean volcanic district | Campi Flegrei-Soccavo 4 | b |
| TM-7-1 | | | 12,590 | 630 | Phlegrean volcanic district | Campi Flegrei-Gaiola | b |
| TM-7-2 | 12,980 | 60 | 12,640 | 630 | Phlegrean volcanic district | Campi Flegrei-La Pigna | b |
| TM-10a | 13,070 | 90 | 15,030 | 750 | Phlegrean volcanic district | Campi Flegrei-Lagno Amendolare | b |
| L7 | 14,000 | 14,000 | | | Phlegrean volcanic district | Campi Flegrei/Unità tefra superiori | d |
| TM-7-3 | 14,900 | 400 | 12,770 | 640 | Phlegrean volcanic district | Campi Flegrei-NYT | b |
| TM-12* | 15,920 | 110–130 | 17,560 | 880 | Somma Vesuvius | Pomici Verdoline | b |
| TM-12–1 | 16,950 | 360 | 17,980 | 900 | Mount Etna | Biancavilla Y-1 | b |
| TM-10-1 | 17,800 | 3200 | 15,820 | 790 | Phlegrean volcanic district | Ischia-St. Angelo | b |
| TM-12–2a | 17,900 | 500 | 18,500 | 920 | Phlegrean volcanic district | Campi Flegrei-Tufi Biancastri | b |
| TM-13* | 18,300 | 180 | 19,280 | 960 | Somma Vesuvius | Pomici di Base | b |
| TM-14 | 19,620 | 270 | 20,150 | | Phlegrean volcanic district | Procida-Solchiaro | a |
| TM-15 | 21,299 | 170 | 23,930 | | Phlegrean volcanic district | Campi Flegrei- Masseria del Monte Y-3 | a |
| L10 | 22,250 | 1000 | | | Somma Vesuvius | Sarno Formation | d |
| TM-16a | 25,100 | 400 | 26,130 | | Somma Vesuvius | Codola (top) | a |
| TM-17a | | | 25,930 | | Albano volcanic district | Peperino Albano Ignimbrite | a |
| L12 | 36,200 | 36,200 | | | Phlegrean volcanic district | Ignimbrite campana Y-5 | d |
| L14 | 55,000 | 55,000 | | | Phlegrean volcanic district | Ischia/Monte Epomeo Tufi Verdi | d |
| TM-20 | 56,000 | 4000 | 57,570 | | Phlegrean volcanic district | Ischia Y-7 | a |
| TM-22 | 79,300 | 4200 | 85,320 | | Pantelleria | Green Tuff Pantelleria P-10 | a |
| TM-23 | 85,000 | 9000 | 85,670 | | Sabatini volcanic district | Tufo di Baccano | a |
| TM-31 | 102,000 | | 114,770 | 5740 | Phlegrean volcanic district | Campi Flegrei | c |
| TM-24a | 105,000 | 2000 | 97,770 | | Phlegrean volcanic district | X-5 (Pumice fallout) | a |
| TM-26 | 106,300 | 5300 | 106,300 | 5320 | Mount Etna | Salto della Giumenta Unit | c |
| TM-29-1 | 111,500 | 5600 | 111,480 | 5570 | Phlegrean volcanic district | Campi Flegrei | c |
| TM-29-2 | 111,500 | 5600 | 112,460 | 5620 | Phlegrean volcanic district | Campi Flegrei | c |
| TM-30-1 | 111,500 | 5600 | 113,370 | 5670 | Phlegrean volcanic district | Campi Flegrei | c |
| TM-30-2 | 111,500 | 5600 | 114,440 | 5720 | Phlegrean volcanic district | Campi Flegrei | c |
| TM-32 | 115,300 | 5800 | 115,250 | 5760 | Aeolian Islands | Stromboli/Petrazza Y-9 | c |
| TM-33-2 | 115,700 | 5800 | 118,190 | 5910 | Phlegrean volcanic district | Ischia/Punta Imperatore | c |
| TM-34 | 118,800 | 5900 | 118,810 | 5940 | Aeolian Islands | Salina | c |
| TM-35a | 120,700 | 6000 | 120,670 | 6030 | Phlegrean volcanic district | Campi Flegrei | c |
| TM-35b | 120,700 | 6000 | 121,940 | 6100 | Phlegrean volcanic district | Campi Flegrei | c |
| TM-37 | 124,100 | 6200 | 124,080 | 6200 | Phlegrean volcanic district | Ischia/Monte di Vezzi | c |
| TM-42 | 132,100 | 6600 | 132,110 | 6610 | Phlegrean volcanic district | Ischia/Scarrupata di Barano | c |

Ohrid (Vogel et al., 2010; Wagner et al., 2008, 2019; Francke et al., 2019; Leicher et al., 2016, 2021) and in Lago di Monticchio (Narcisi, 1996; Wulf et al., 2004, 2008, 2012). The lacustrine sequences of these two lakes appear to be the most representative archive for the recognition of tephra layers in the Mediterranean area. In fact, they preserve various volcanic products coming from the volcanoes of Campania but, being at two very different distances from the volcanic source of Somma Vesuvius, they present a different tephra content of this particular volcano. Lago di Monticchio is located about 100 km from the Somma Vesuvius, and for this reason it appears to be an excellent database for the recognition of its tephra. Within this core sample, tephra from explosive eruptions between 79 CE and 132,100 years ago were identified (Table 2). Lake Ohrid, on the other hand, is located about 530 km from Somma Vesuvius, therefore, within this core sample, layers were verified only relating to large magnitude eruptions originating from the Neapolitan volcanic district. Notably, in this case the tephrostratigraphic succession of Lake Ohrid extends from 1.46 ± 0.02 ky to 1221.57 ky (Table 3).

## 2. Methods

The goal is to define a simplified method to produce probability maps that a given target location is reached by a particular grain size of tephra, provided that an eruption of a certain size occurs at a given volcano. These maps should include the far field of the volcano, without requiring an explicit calculation of tephra dispersal over such large areas. To this end, the method considers in input only the intensity and direction of winds in the last 30-years, the different heights of the

**Table 3**
Core of the Lake Ohrid. Reference: a) Leicher et al., 2016; b) Leicher et al., 2021; c) Leicher et al., 2021; d) Wagner et al., 2019; e) Francke et al., 2019; f) Vogel et al., 2010.

| Tephras | Age (yr BP) | | Volcanic district | Eruption | References |
|---|---|---|---|---|---|
| | Data | (±) | | | |
| OH-DP-0009 | 1.46 | 0.02 | Somma Vesuvius | 472/512 CE | d |
| OH-DP-0015 | 3.37 | 0.07 | Mount Etna | FL | d |
| OH-DP-0016.2* | 3.61 | 0.1 | Somma Vesuvius | AP1-AP2 | e |
| OH-DP-0019.2* | 4.5 | 0.2 | Phlegrean volcanic district | CF-Agnano Monte Spina | |
| OH-DP-0026.* | 8.2 | 0.3 | Aeolian Islands | Gabellotto-Fiumebianco (Lipari) | |
| OH-DP-0027 | 8.43 | | Somma Vesuvius | Pomici di Mercato | a |
| OH-DP-0049 | 14.75 | 0.52 | Phlegrean volcanic district | Campi Flegrei LN2 | d |
| OH-DP-0052* | 15.53 | 0.62 | Phlegrean volcanic district | Campi Flegrei LN1 | d |
| OH-DP-0115 | 28.68 | | Phlegrean volcanic district | Campi Flegrei-Masseria del Monte | c |
| OT0702–5 | 34.27 | 0.87 | Somma Vesuvius | Codola | f |
| OH-DP-0169 | 39.95 | 0.12 | Phlegrean volcanic district | Campi Flegrei/Ignimbrite Campana | a |
| OT0702–7 | 46.9 | 3.6 | Phlegrean volcanic district | Green Tuff Pantelleria? | f |
| OH-DP-0435 | 109.5 | 0.9 | Phlegrean volcanic district | Campi Flegrei X-6 | a |
| OH-DP-0499 | 133.5 | 2 | Pantelleria | | a |
| OH-DP-0505 | 135.36 | 4.06 | Pantelleria | | b |
| OH-DP-0599 | 156.89 | 3.79 | Vicano-Cimino Volcanic District | Vico B | b |
| OH-DP-0616 | 158.76 | 3.83 | Vicano-Cimino Volcanic District | Vico B | b |
| OH-DP-0617 | 163 | 22 | Vicano-Cimino Volcanic District | Vico Ignimbrite B | a |
| OH-DP-0624 | 158.29 | 3 | Vicano-Cimino Volcanic District | Vulcano Vico D | a |
| OH-DP-0710 | 172.26 | 5.5 | Phlegrean volcanic district | Campi Flegrei-Acqua Feconia | a |
| *OH-DP-0725** | 174.44 | 5.22 | Pantelleria | | not published |
| OH-DP-0766 | 180.02 | 4.14 | Pantelleria | | b |
| OH-DP-0997 | 228.87 | 5.66 | Phlegrean volcanic district | Roccamorfina? | b |
| OH-DP-1006 | 230. 93 | 6.27 | Phlegrean volcanic district | Ischia-Taurano Ignimbrite? | b |
| OH-DP-1055 | 240.93 | 6.45 | Phlegrean volcanic district | Ignimbrite Seiano? | b |
| OH-DP-1175 | 270.64 | 4.88 | Sabatini volcanic district | | b |
| OH-DP-1513 | 353.43 | 7.49 | Aeolian Islands | | b |
| OH-DP-1520 | 355.76 | 7.64 | Aeolian Islands | | b |
| OH-DP-1527 | 358. 25 | 4.64 | Roccamorfina district | Roccamorfina | b |
| OH-DP-1640 | 398.37 | 5.95 | Roccamorfina district | Roccamorfina | b |
| OH-DP-1700.6 | 410 | 2 | Vicano-Cimino Volcanic District | Vico Ignimbrite B | d |
| OH-DP-1719.7* | 419.76 | 5.41 | Sabatini volcanic district | Monti sabatini | not published |
| OH-DP-1733 | 423.93 | 6.43 | Roccamorfina district | Roccamorfina | b |
| OH-DP-1812 | 453.95 | 2.94 | Roccamorfina district | Roccamorfina | b |
| OH-DP-1817 | 456.19 | 3.3 | Albano volcanic district | Pozzolane Rosse | b |
| OH-DP-1911 | 480.49 | 6.84 | Sabatini volcanic district | | b |
| OH-DP-1955 | 490.67 | 3.92 | Sabatini volcanic district | Tufi Terrosi | a |
| OH-DP-1966 | 494. 05 | 4.43 | Roccamorfina district | Roccamorfina | b |
| OH-DP-1998 | 508.67 | 4.14 | Vulsini volcanic district | | b |
| OH-DP-2010 | 514.17 | 4.37 | Sabatini volcanic district | Fall A | a |
| OH-DP-2017 | 516.87 | 5.47 | Phlegrean volcanic district | CVZ | a |
| OH-DP-2060 | 530.86 | 3.35 | Albano volcanic district | Tufo Bagni Albule | a |
| OH-DP-2439 | 626.87 | 3.98 | Mount Vulture | | b |
| OH-DP-2512 | 648.56 | 6.76 | Phlegrean volcanic district | CVZ | not published |
| OH-DP-2555 | 662.55 | 7.16 | Phlegrean volcanic district | CVZ | not published |
| OH-DP-2589 | 674.22 | 5.93 | Mount Vulture | | not published |
| OH-DP-2603 | 680.85 | 4.46 | Phlegrean volcanic district | CVZ | not published |
| OH-DP-2669 | 717.3 | 5.4 | Phlegrean volcanic district | CVZ | d |
| OH-DP-2717 | 734.41 | 5.86 | Roccamorfina district | | c |
| OH-DP-2869 | 776.51 | 5.14 | Phlegrean volcanic district | CVZ | not published |
| OH-DP-2898 | 791.9 | 1.9 | Roccamorfina district | | c |
| OH-DP-3144 | 888.18 | 5.28 | Phlegrean volcanic district | CVZ | not published |
| OH-DP-3443 | 979.32 | 6.19 | Phlegrean volcanic district | CVZ | not published |
| OH-DP-3860 A + B | 1113.67 | 7.36 | Phlegrean volcanic district | CVZ | not published |
| OH-DP-3914 | 1132.57 | 4.27 | Phlegrean volcanic district | CVZ | not published |
| OH-DP-4089 A + B | 1206.89 | 4.55 | Phlegrean volcanic district | CVZ | not published |
| OH-DP-4124 | 1221.57 | 6.49 | Phlegrean volcanic district | CVZ | not published |

eruptive column, and the maximum distance that tephra can travel in different wind conditions. This allows the creation of a simplified dispersal model, which enables associating to a given grain size the probability to be found at a given place.

To accomplish this objective, wind characteristic data were downloaded and analysed from the online re-analysis database Climate Data Store-Copernicus (Earth Rapidly Acquired 5th- ERA5). These data provide hourly estimations of a variable number of atmospheric, terrestrial and oceanic meteorological parameters. Wind data were downloaded at the following pressure levels: 1, 2, 3, 5, 10, 20, 50, 100, 300, 500, and 1000 hPa (corresponding to heights from 30 km to 0.1 km). Wind data was downloaded for each day from 1990 to 2020 at 6:00 AM and 6:00 PM, resulting in a total of 21,900 records. Based on the wind data, it can be observed that in the central Mediterranean area there is a predominant wind component from west to east, common for these latitudes. For eruptive columns of 20 km and 30 km, there is also a wind component from east to west, but with lower intensity. For heights below 10 km, the characteristics of wind intensity and direction are more variable, although the west to east component remains prevalent.

The time span considered in this study mainly covers eruptions of the last 10,000 years, with only two cases up to 20,000 years (Base Pomici and Verdoline Pomici). For this reason, we consider the one made on

wind data to be a reasonable approximation, since the basic structure of the atmospheric circulation has not been dramatically altered, comparing the atmospheric conditions during the Last Glacial Maximum with today's conditions (Lautenschlager and Herterich, 1990).

To determine the distances that the various tephra grain sizes may reach, we used results from HAZMAP simulations (Macedonio et al., 2005; Costa et al., 2013). HAZMAP is a model used to solve the diffusion, transport and sedimentation equations of small particles and model the ash dispersion generated by a sustained convective column (Macedonio et al., 2005). These simulations do not depend on the specific target area, but only on the typical wind profiles at different latitude ranges (equatorial, mid-latitude and polar) (Costa et al., 2016). The Eruption Source Parameters (ESP) that were used for the simulations are the values of the column heights and the mass of the fall-out pyroclastic products. In fact, no ESP was set starting from the data of the two reference targets, Lago di Monticchio and Lake Ohrid. A total of 18 simulations were performed in HAZMAP, 9 for the 4ϕ grain size and 9 for the aggregate grain size. These simulations were produced under light, medium and strong wind conditions and for eurtive columns of 10, 20 and 30 km.

The developed method is initially applied to Somma Vesuvius, but it is applicable everywhere to any eruptive source in the same area. We defined a target grid within a range of 5–37 degrees longitude and 29–44 degrees latitude (Fig. 1b), and a nodal distance of 0.1 degrees latitude and longitude (about 11 km). Obviously, we implicitly assume that the wind is uniform within such a large domain, that is typically not valid but, since we are interested to the daily average and on a statistical treatment, we can maintain such a simplification (Sandri et al., 2016; Matthews et al., 2015) and improve the method in future works by using 3D time-dependent wind fields which require intense HPC resources (see e.g., Martínez et al., 2022; Massaro et al., 2023).

To define the best approach to quantify the probability maps, we implemented three methods, with increasing sophistication:

1) Method A (SA_phi4): we used HAZMAP simulations for the grain size of 0,063 mm (4 $\phi$) and a vertically uniform wind equal to that blowing at top of column height, considering three distinct eruptive size classes (10, 20, and 30 km).
2) Method B (MA_phi4): like Method A, but sampling wind intensity and direction from the elevation 0.1 km to the upper part of the eruptive column (from 0.1 to 10 km, from 0.1 to 20 km and from 0.1 to 30 km).
3) Method C (MA_agg): like Method B but using aggregated particles instead of $\phi = 4$.

### 2.1. Quantification of the probability of Method a (Sa_phi4)

For a given target point $\boldsymbol{x}$ = (lat, lon) and a given grain size, we quantify the probability that $\boldsymbol{x}$ is reached by the tephra of grain size $\phi$ generated by a source in $\boldsymbol{x_s}$ as:

$$P_A(x|x_s, h_c, \phi_A) = P(\theta|h_c)P(v_{ref})P(d(x, x_s)\,|v_{ref}, \phi, h_c) \quad (1)$$

where $\theta$ represents the angle to the north of the line connecting source $x_s$ and target $x$; $h_c$ the column height; $d(x, x_s)$ their distance between $\boldsymbol{x}$ and $\boldsymbol{x_s}$; $P(\theta|h_c)$ and $P(v_{ref})$ are the probability of having at the target a wind blowing sufficiently close to $\theta$ at the altitude $h_c$ and with a maximum velocity of the profile larger than $v_{ref}$; $P(d(x, x_s)\,|v_{ref}, \phi, h_c)$ is the probability that a given $\phi$ will cover the distance $d$, given a wind with velocity $v_{ref}$. Following Costa et al. (2016), the maximum velocity of the profile $v_{ref}$ is calculated at the tropopause altitude, that is 12 km at our latitudes.

To compute $P(\theta|h_c)$ and $P(v_{ref})$, we considered the distribution of wind profiles at the source. Here, we use the coordinates of Somma Vesuvius. However, wind profiles are similar to each other in the same area, especially for the higher altitudes, making tephra fall hazard from sub-Plinian and Plinian columns, relatively insensitive to the exact

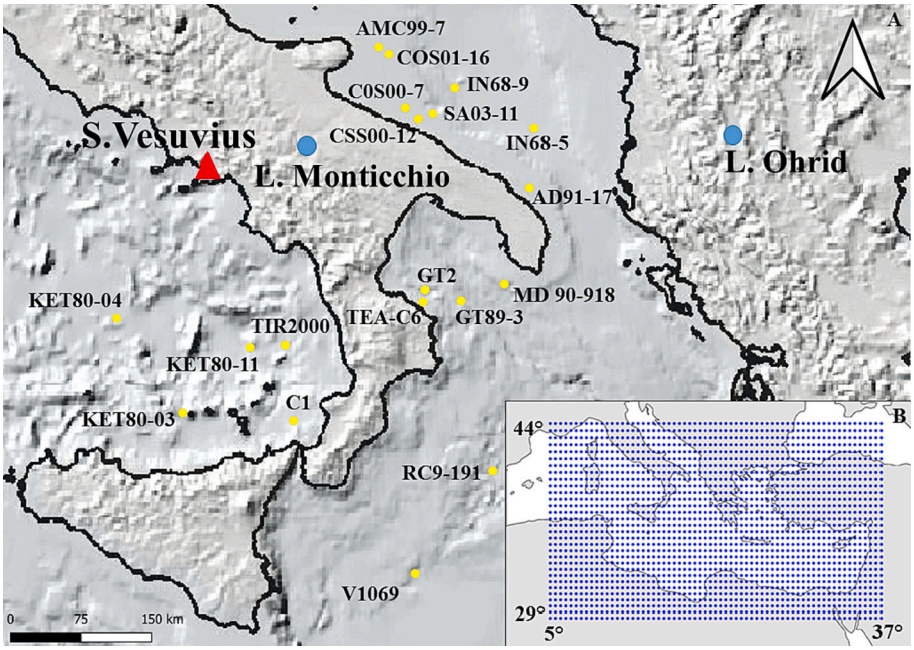


**Fig. 1.** in Fig. 1a, the eruptive source and the corings present in the Mediterranean area are depicted: the Somma Vesuvius volcano is represented by the red triangle; the two primary cores under consideration, located in the Lake of Monticchio and Lake Ohrid, are indicated by the blue dots; the yellow dots denote all other corings in the Mediterranean area, primarily utilized for the LOGIT validation exercise (Kereszturi et al., 2017; Ang et al., 2020). In Fig. 1b, on the other hand, the entire area from which the data concerning wind intensity and direction characteristics between 1990 and 2020 were sourced is illustrated (Paterne et al., 1988; Di Roberto et al., 2008; Insinga et al., 2019; Keller et al., 1978; Di Donato et al., 2019; Crocitti et al., 2018; Castagnoli et al., 1990; Caron et al., 2012; Marchini et al., 2014; Calanchi et al., 2008; Lowe et al., 2017; Siani et al., 2004; Matthews et al., 2015; Jalali et al., 2018; Narcisi et al., 1996; Wulf et al., 2004, 2008, 2012; Wagner et al., 2019; Leicher et al., 2016, 2021; Vogel et al., 2010).

location of the retrieval of the wind (Selva et al., 2013). Thus, if we assume negligible or we correct for potential topographic effects, this evaluation results a good statistical approximation for all volcanoes of the area.

All data are here averaged over areas of 0.1 by 0.1 degree (11 × 11 km) (Fig. 1b). Using ERA5, we recovered the geopotential variables, $u$ and $v$ components, which are the zonal and southern wind components respectively. In evaluating $P(\theta|h_c)$ and $P(v_{ref})$, a tolerance of 30 degrees on $\theta$ and of 15% on $v_{ref}$ were considered. In other words, for any angle $\theta$, $P(\theta|h_c)$ was calculated by counting the number of times the wind had a direction at the top of the column within $\theta \pm 15$ degree and dividing by the number of records. Similarly, for any velocity $v_{ref}$, $P(v_{ref})$ was calculated by counting the number of times the wind had a speed larger than $v_{ref}$ less 15% at an altitude of 10 km and dividing by the number of records. To assess $P(d(x,x_s)\,|v_{ref},\phi,h_c)$, we have to consider the distances that various grain sizes of tephra can travel under typical wind conditions and column heights. These values were based on wind profiles at medium latitudes and under weak, medium, and strong wind conditions. To determine the maximum reachable distances, 9 HAZMAP simulations were used to determine the distances that a tephra can cover in weak, medium, and strong wind conditions (7, 30, and 70 m/s; Costa et al., 2016) and with column heights of 10, 20 and 30 km, depositing a thickness of at least 0.1 mm (representative of a cryptotephra). In this way, we obtained a total of 9 distance values (in km) for each column height (10, 20, and 30 km) and wind speed (7, 30, and 70 m/s). For each column height, the distances relative to the three wind speeds considered (7, 30, and 70 m/s) are linearly interpolated, to obtain the values of the intermediate wind speeds, at each point of the grid. Then, the probability $P(d(x,x_s)\,|v_{ref},\phi,h_c)$ for that wind field was treated as a step function at the maximum distance achievable for any given velocity $v_{ref}$, that is equal to 1 if $d$ is smaller than the maximum distance, and 0 otherwise. This was repeated for each wind field to convert the step functions into probabilities.

With this information, the probabilities that the grain size $\phi_4$ can reach a given distance from the eruptive source are calculated for each point of the grid. The results are reported in Figs. 2a, 2b, 2c.

### 2.2. Quantification of the probability of Method B (Ma_phi4)

This group considers the contribution of winds at all altitudes up to the top of the column height. Since wind directions are statistically correlated at the different altitudes, we assume a full correlation among the different wind intensities and velocities. Therefore, Eq. (1) becomes:

$$P_B(x|x_s,h_c,\phi_A) = \left(P(\theta|h)P(v_{ref})P(d(x,x_s)\,|v_{ref},\phi,h)\right) \quad (2)$$

The expression inside the maximum is equal to the one of Eq. (1), but the direction of the wind and the maximum distance reached by the tephra are calculated at all the intermediate altitudes instead of only the top of the column, then taking the maximum among them for each target point. This should benefit the quantification in the near intermediate distances, where the potential contribution of intermediate altitudes may be relevant. As discussed above in Method A, the velocity is instead always retrieved at the reference altitude of 10 km.

For group B, we consider 32 pressure levels ranging from 10 hPa to 1000 hPa, corresponding at 0.1, 0.3, 0.5, 0.75, 0.9, 1.2, 1.4, 1.6, 1.9, 2.2, 2.4, 3, 3.5, 4.2, 4.8, 5.5, 6, 9, 10, 11, 11.8, 12.5, 13.5, 14, 15, 17, 19, 21, 23, and 30 km. The HAZMAP simulations produced for three column heights, but now we want to consider also the dispersion of intermediate levels of the column. To this end, we first interpolate for the intermediate eruptive column levels (32 wind levels), and then for intermediate wind speeds. The obtained values were used to evaluate $(d(x,x_s)\,|v_{ref},\phi,h_c)$. The results are reported in Figs. 2d, 2e, 2 f.

### 2.3. Quantification of the probability of Method C (Ma_agg)

As regards the third and last group of maps (MA_agg), the entire procedure described for the maps of group B was followed, but for particles created by aggregating different grain size classes of fine ash, called "agg". HAZMAP simulations were carried out using this effective grain size class. Also in this case the total dependence of the winds at the different altitudes is taken into account. Therefore, for all the points of the grid, the maximum probability values, associated with the grain size of the aggregates were calculated using this formula:

$$P_C(x|x_s,h_c,\phi_A) = (P(\theta|h))P(v_{ref})P(d(x,x_s)\,|v_{ref},\phi_A,h)) \quad (3)$$

Which is identical to Eq. 2, with the use of another grain size class. For the class of aggregates $\phi_A$ we considered the parameterization of Cornell et al. (1983), which assumes that the particle sizes of the aggregates are composed either of 50% of ash with diameters 63–44 μm, or of 75% of 44–31 μm, or for 100% of particles <31 μm, forming aggregates with a diameter of 200 μm and a density of 400 kg $m^{-3}$ (Folch et al., 2010). However, the terminal velocity of this class corresponds to an effective settling velocity of the order of 0.3–0.4 m/s (Costa et al., 2010). The results are reported in Figs. 2 g, 2e, 2 h for the three selected $h_c$.

## 3. Result

### 3.1. Probability maps

In Fig. 2a, the probability maps obtained by Method A show the probabilities of finding a deposit with a particle grain size of 0.063 mm ($\phi = 4$) at various distances from the eruptive source during an eruption with a 10 km eruption column. The maximum probabilities are always eastward, with 40% at around 170 km, 20% at 510 km and 1% at 740 km from the source. For column height of 20 km (Fig. 2b), 40% at 180 km, 20% at 535 km and 1% at 800 km from the source. There is a westward component of the probability with a maximum probability of 20% at 180 km and 1% at 350 km. For a column height of 30 km (Fig. 2c), the maximum probability of 40% at 190 km, 20% probability at 890 km, and the 1% at 1380 km from the source. Also in this case, there is a westward component of the probability, which reach a maximum of 30% at 400 km and 1% at 750 km.

Adopting Method B, considering the 10 km eruptive column, the maximum probability is 40% at 315 km from the source, 20% at 695 km and 1% at 800 km (Fig. 2d). For an eruption column of 20 km, the maximum probability of 60% at 250 km, 40% at 555 km, 20% at 805 km and 1% at 920 km. The western component shows probability of 20% at 180 km and 1% at about 380 km (Fig. 2e). The case of 30 km eruptive column (Fig. 2 f) shows the probability of 60% at 270 km, 40% at 560 km, 20% at 1020 km and 1% at 1585 km. The western component shows probability of 30% at 410 km and 1% at about 860 km.

For Method C, Figs. 2 g, 2 h, and 2i show the values of maximum probability for aggregate volcanic particles. For 10 km column (Fig. 2 g), the probability values are 40% at 225 km, 20% at 485 km and 1% at 560 km. In the case of 20 km eruptive column (Fig. 2 h) we have 60% probability at 170 km, 40% at 350 km, 20% at 520 km and 1% at 580 km. Fig. 2i shows the probability maps for 30 km eruptive column, with a probability of 60% at 190 km, 40% at 360 km, 20% at 675 km and 1% at 985 km. For both 20 km and 30 km columns (Fig. 2 h and Fig. 2i), there is also an east-west wind component. In this wind direction, the probabilities get to be 1% at 150 km for the 20 km eruptive column, and at 570 km for 30 km eruptive column. All the maps show an almost linear decrease of maximum probability (in respect to the different angles) with distance, testifying for the first order approximation of the produced maps. Furthermore, as a result of the modelling choices and the way in which the variables are used within the method, it can be noted that to the north and south of the eruptive vent, in all the maps,

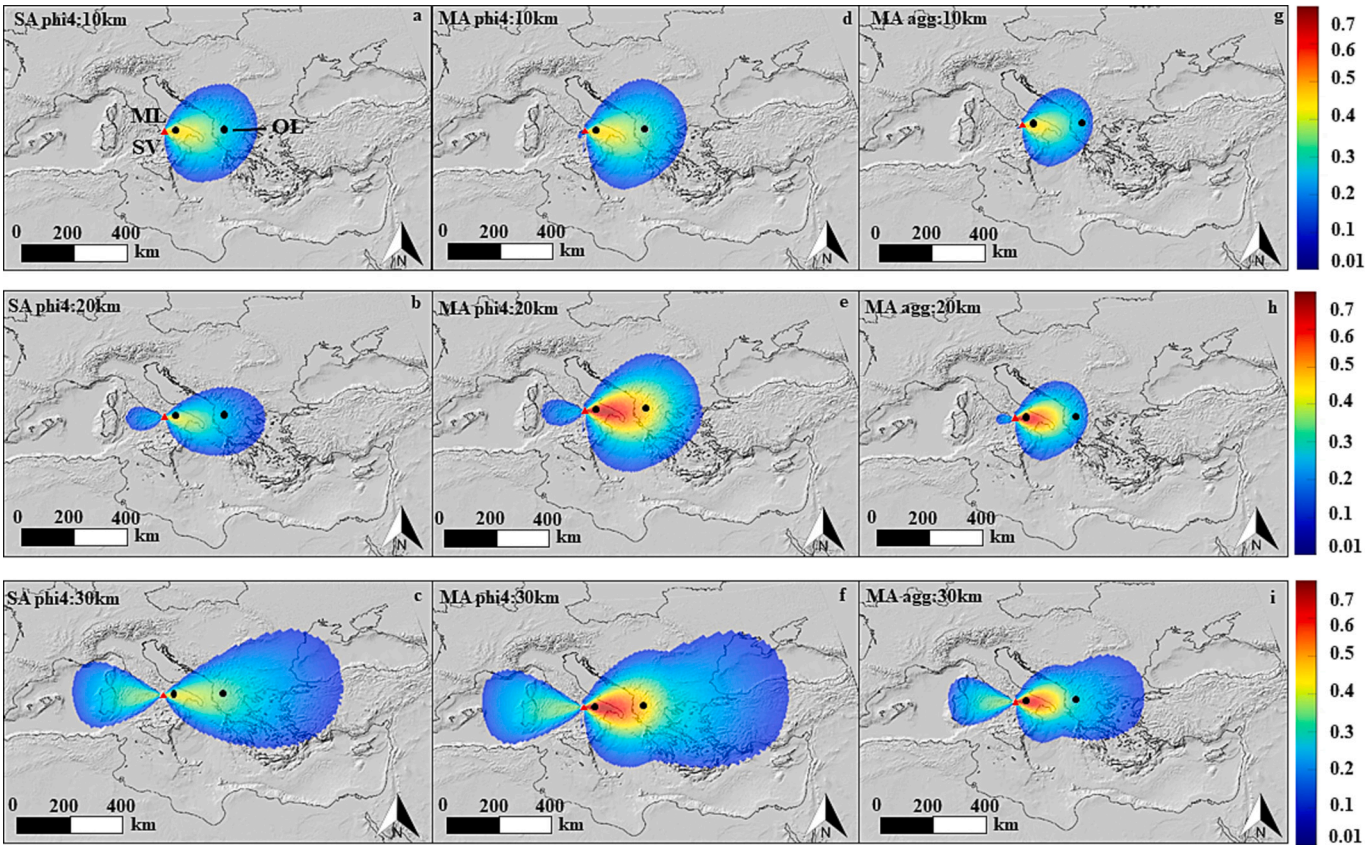


**Fig. 2.** probability maps. SV: Somma Vesuvius; ML: Monticchio Lake; OL: Ohrid Lake. Fig. 2a, 2b, 2c refer to the SA_phi maps respectively relating to the columns of 10, 20 and 30 km. Fig. 2d, 2e, 2 f refer to the MA_phi maps respectively relating to the columns of 10, 20 and 30 km. Fig. 2 g, 2 h, 2i refer to the MA_agg maps respectively relating to the columns of 10, 20 and 30 km. The Somma Vesuvius volcano is marked with the red triangle. The two main cores considered present in the Great Lake of Monticchio and in the Ohrid Lake are marked with the black dots.

the probabilities present values <1%. The SA_phi4 maps show a linear decrease of maximum probability with distance (Fig. 2a, 2b, 2c), with column heights of 10 km and 20 km that show quite similar decay and close values of probability (Fig. 3a). The probability of 30 km column height shows a gentler decrease with respect to the other two (Fig. 3a). This behaviour clearly reflects the dependence of probability from column heights and wind patterns.

### 3.2. Model validation and method selection

The selection of the appropriate method among the 3 alternatives discussed can be made through a validation study using the observed frequencies at two target locations with a particularly well recorded tephrostratigraphy: Lago di Monticchio and Lake Ohrid (Fig. 2a, 2b, 2c; Table 4). In these locations we can compare the computed probabilities with the observed frequencies for the three reference sizes in the recent activity of Somma Vesuvius, which is known from proximal records. The frequencies observed, as reported in Table 4, at Lake Monticchio, are 0 tephra associated with the 10 known eruption with approximately 10 km eruptive columns (observed frequency 0%), 7 tephra relating to the 9 known eruption with 20 km eruptive columns (observed frequency 78%) and 3 tephra connected to the 3 known eruptions with 30 km eruptive columns were verified (100%). At Lake Ohrid, the tephra observed in the core sampling are 0 relating to the 10 eruptions with 10 km eruptive columns (0%), 3 tephra relating to the 9 eruptions with 20 km eruptive columns (33%), and 0 tephra relating to the 3 eruptions with 30 km eruptive columns (0%).

Considering Method A, it can be seen how, for the Lago di Monticchio data, there is not a good agreement for the 10 km column (35% probability vs 0% observed; Table 4), nor for the 20 km column (29% probability vs 78% observed) and from 30 km (40% probability vs 100% observed). At Lake Ohrid the discrepancies are 19% versus 0% for the 10 km column, 32% versus 33% for the 20 km column, and 42% versus 0% for the 30 km column. Even if we consider the possible bias due to not complete recognition of tephra layers in distal areas, the unsatisfactory match between calculated probabilities and observed distances indicate the SA_phi4 method is probably too simplified and tends to overestimate the distance traveled by ash particles.

Method B (Ma_phi4), including the intermediate levels, increases the probabilities in proximal areas, reaching values close to 60% within the first 250 km from the eruptive source. The 10 km column increases the maximum distance of 20% probability of 36% (from 510 km to 695 km; Fig. 3b), while the 20% probability increases the maximum distance of ca. 50% for the 20 km column (from 535 km to 805 km), and 15% for the 30 km column (from 890 km to 1020 km; Fig. 3b). These results highlight the importance of lower atmosphere winds in the dispersal of tephra, especially for low-height columns (Fig. 4). When comparing the probabilities with real data for Lago di Monticchio, we have an apparent worsening of match for the 10 km column (43% probability vs 0% observed frequency) and a significant improvement for 20 km column (64% probability vs 78% observed frequency) and 30 km column (65% probability vs 100% observed frequency). Comparing to Lake Ohrid data we again have poor matches for all the considered eruptive columns, with 31% probability vs 0% real for 10 km column, 46% probability vs 33% real for 20 km column and 47% probability vs. 0% real for 30 km column. Also in this case therefore, the MA_phi4 maps seem to overestimate the distances traveled by the tephra particles.

A more quantitative comparison can be made considering that the expected number of observations (i.e. the number of tephra that should be found within the core samples; Table 4) can be considered an

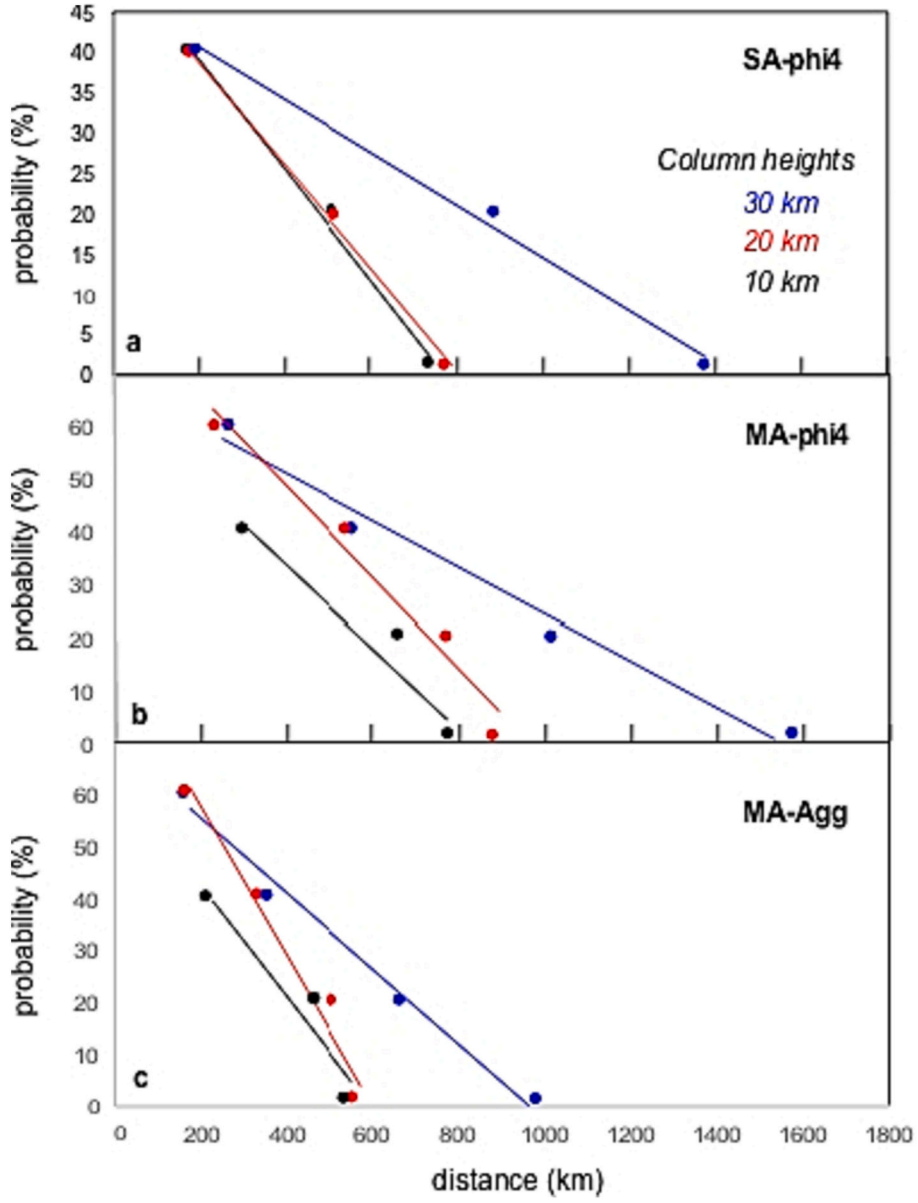


**Fig. 3.** These graphs allow us to define the relationships between probability values and distances for each type of map and for each column height considered. Fig. 3a considers the case of SA_phi4 maps, Fig. 3b the MA_phi4 maps and Fig. 3c the MA_adj maps.

**Table 4**
Probability values related to the SA_phi4. MA_phi4. and MA_agg maps are divided based on the different heights of the eruptive columns. The quantities of tephra found in the core drillings of Lake Monticchio and Lake Ohrid are also included. Along with the total number of eruptions from Somma Vesuvius. categorized according to the eruptive column heights. In Section 3, we propose 3 alternative configurations for the model.

| | SA_phi4 | | MA_phi4 | | MA_agg | | | | |
|---|---|---|---|---|---|---|---|---|---|
| Eruptive column (km) | Probability | | Probability | | Probability | | N° tephras | | N° eruption |
| | L. Mont | L. Ohrid | L. Mont | L. Ohrid | L. Mont | L. Ohrid | L. Mont | L. Ohrid | |
| 10 | 0.35 | 0.19 | 0.43 | 0.31 | 0.43 | 0.23 | 0 | 0 | 10 |
| 20 | 0.29 | 0.32 | 0.64 | 0.46 | 0.64 | 0.26 | 7 | 3 | 9 |
| 30 | 0.4 | 0.42 | 0.65 | 0.47 | 0.65 | 0.3 | 3 | 0 | 3 |

independent sampling from the probability map, that is, they should follow a binomial distribution with parameters $p$ and $n$, where $p$ is the probability of the observation (the values relating to the probabilities of finding a tephra at a certain distance from the eruptive source, based on the different eruptive columns identified in Lake Ohrid and Lago di Monticchio; Table 4) and $n$ is the number of trials (the total number of Holocene eruptions of Somma Vesuvius, with a particular eruptive column; Table 1). Therefore, the binomial distribution can be used to test the probability values by evaluating how likely the observations results are if the model is correct (Bebbington, 2013; Selva, 2013; Grezio et al., 2017). To therefore test these probability values and be able to use the maps constructed (Fig. 2), we assume substantial stationarity of the

wind field starting from the Pomici di Base eruption (22 ka; Bebbington and Lai, 1998). In order for the models not to be rejected by binomial distribution test (Grezio et al., 2017), we expect that the probability to record the observed number of tephra layers should larger than a given significance level, which is usually set to 0.05 or 0.01 in standard hypothesis testing. We apply this method to methods B and C.

The results show that Method B cannot be rejected for both lakes in case of 20 km and 30 km eruptive columns (Fig. 5b, c, e, f).

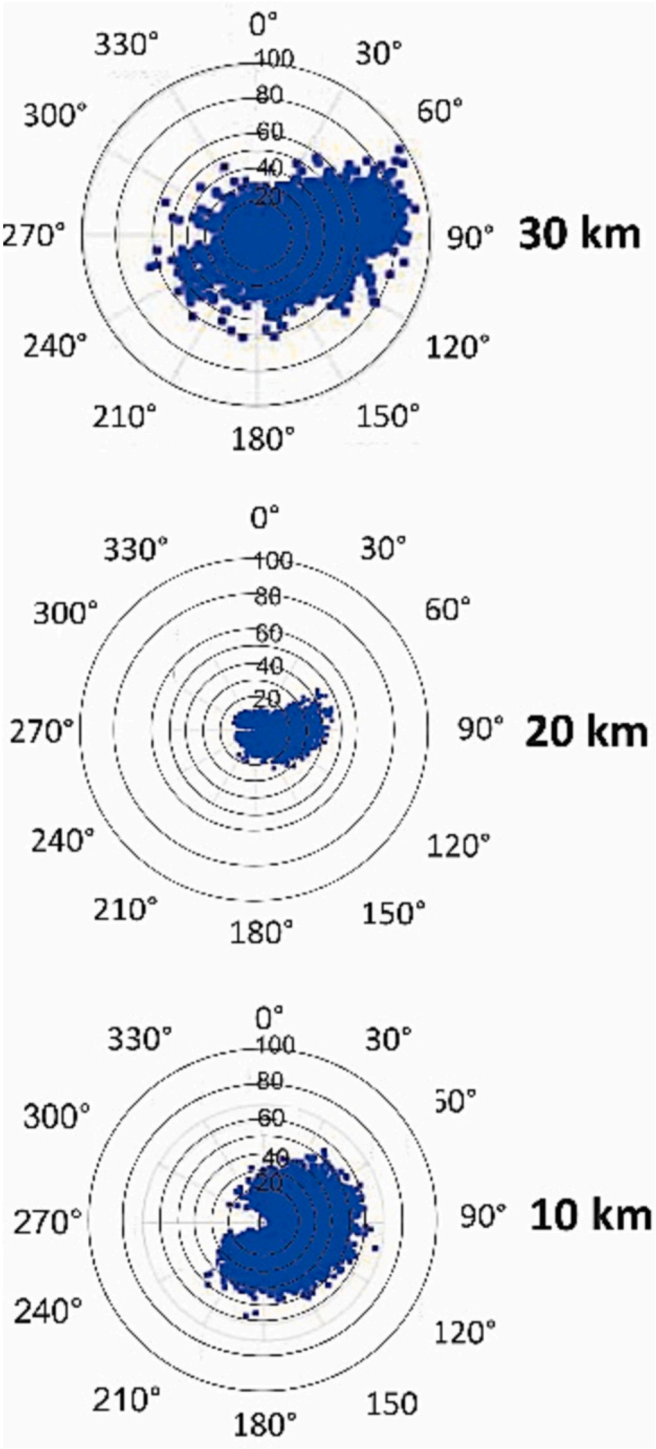


**Fig. 4.** Wind distribution diagrams that allow viewing the different characteristics of intensity and direction at different altitudes (10–20-30 km). For all three cases, the wind characteristics were downloaded over a period of time between 1990 and 2020 from the Climate data Store database.

Discrepancies become apparent regarding the distribution of the 10 km eruptive columns (Fig. 5a, d), for which Method B is rejected in Lago di Monticchio and close-to-rejection (*p*-value between 0.01 and 0.05) in Ohrid. This inconsistency could potentially be attributed to the fact that the height of the eruptive column for the eruption of the Santa Maria Cycle (172–305 CE) was roughly estimated only through the value of the erupted volume (Cioni et al., 2008). The Santa Maria Cycle was divided into 4 eruptions (172 CE, 203 CE, from 222 to 235 CE, and 305 CE), to which only Cioni et al. (2008) estimated only the total volume equal to 0.15 $km^3$ (VEI 3). The 10 km eruptive column was subjectively associated with this volume value. Including the Santa Maria Cycle, there are 10 eruptions of Somma Vesuvius with an eruptive column of 10 km. However, no tephra from Holocene eruptions of Somma Vesuvius with an eruptive column height of 10 km was found inside the two lake cores, although the maps indicate probable values between 30% and 40%. If these 4 eruptions were not considered, the Holocene eruptions of Somma Vesuvius would be reduced to 6, and the results would be more acceptable.

Method C (MA_agg) arises from the fact that, especially in the medial area, ash usually does not fall as single particles but as aggregates, due to the clustering effect due to both atmospheric humidity and forces electrostatics (Cornell et al., 1983; Costa et al., 2010; Brown et al., 2012; Vecino et al., 2022). The aggregate particles can have a greater terminal velocity with respect to the single finer particles, and this reduces the travel distance of fine ash. In order to evaluate the aggregation effect on ash dispersal, we produced the MA_agg maps (Fig. 2 g, 2 h, 2i). The use of aggregation reduces the 20% maximum probability distance of 30% for the 10 km column, 35% for the 20 km column and 51% for the 30 km column (Fig. 3c). When comparing the Method C (MA_agg) probabilities with the Lago di Monticchio data, it emerges how they remain the same than for the Method B (MA_phi4 maps).

Therefore, the results relating to the binomial test are also identical to those already described for the MA_phi4 maps (Fig. 5a, b, c). What changes significantly is the probability for Lake Ohrid, which is 23% probability versus 0% for the 10 km column, 26% versus 33% actual for the 20 km column, and 30% probability versus 0% real for the 30 km column (Fig. 5g, h, i). It can therefore be deduced that the good correspondence shown by the 20 km and 30 km columns indicates how the particle aggregation process affects taller columns. In the binomial test, the p-value for 0 observations in Lake Ohrid increases significantly for Method C to a value larger than 0.05. Therefore, Model C passes the test in Ohrid also for 10 km column height.

In conclusion, a slight preference to Model C is found considering Ohrid lake data. However, the difference between Method B and Method C performances is very small, and we are unable to discriminate well among them. To extend the validation, we need to consider more observations and a more sophisticated statistical approach, as described in the next section.

### 3.3. *Binary logistic regression*

To further investigate the difference between the three methods, and check that the model encapsulates all the relevant factors, we perform another validation test applying a binary logistic regression (Kereszturi et al., 2017; Ang et al., 2020) to the MA_phi4 and MA_agg maps. To do this we consider the observed deposition of volcanic particles in the proximal and distal areas with respect to the eruptive source, based on the tephras actually found in marine and lake cores, comparing these yes/no observations with the calculated probabilities from the maps.

Binary logistic regression variables (Davis et al., 2002) is a statistical model used to assess the connection between a (predicted, or dependent) categorical variable that has only two possible outcomes, and one or more (predictor, or independent) variables that can be continuous or categorical. The only definite information about a given tephra at a given location is whether or not it can be found. Hence our dependent variable has two levels, observed (1) or not observed (0).

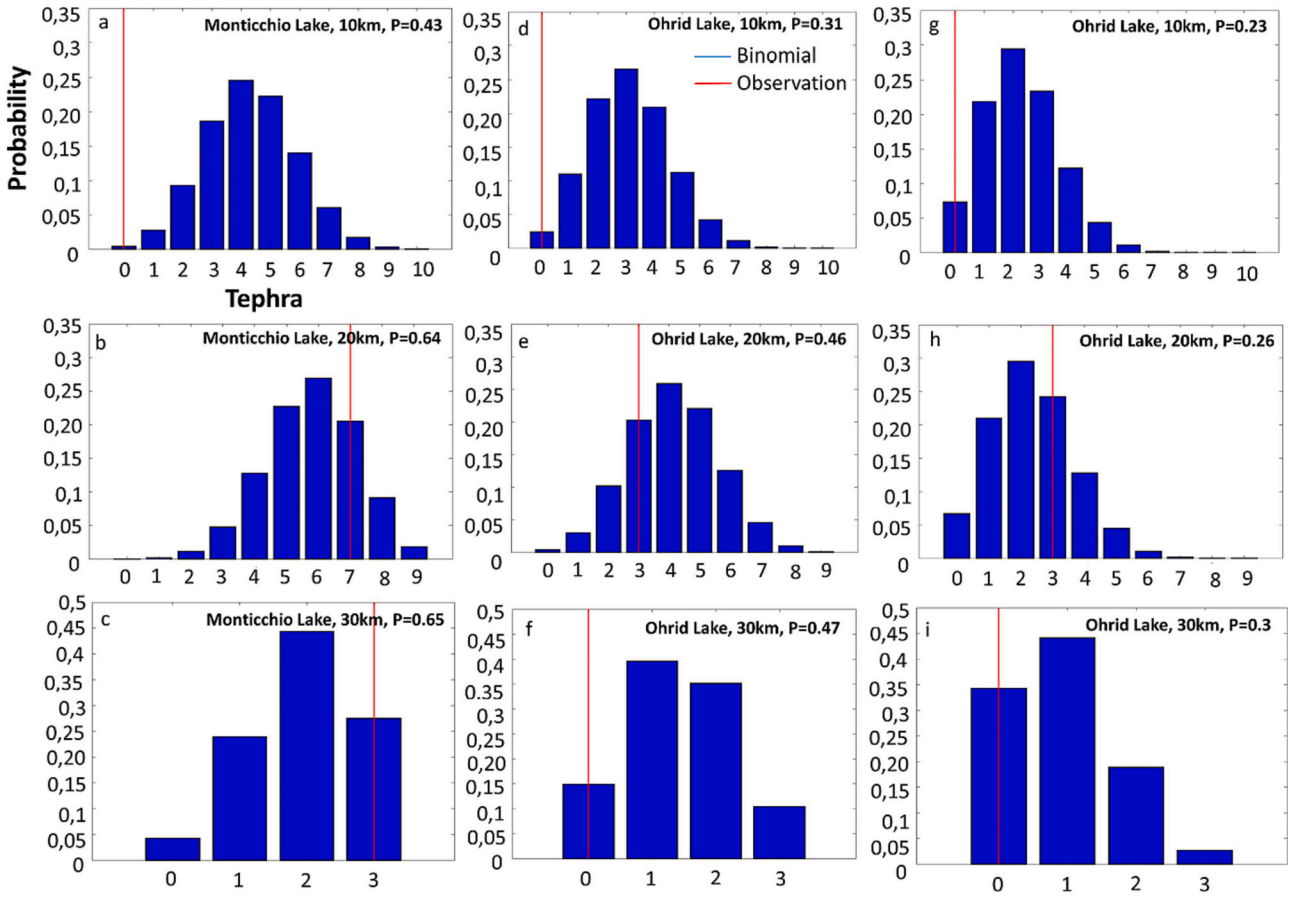


**Fig. 5.** Plots of binomial distributions broken down by different probability values. Fig. 5a, b, c refer to the probability values relating to Lago di Monticchio both for both Method B(MA_phi4) and for Method C (MA_agg), as the have equal probabilities. Fig. 5d, e, f refer to the probability values related to Lake Ohrid for Method B (MA_phi4). Fig. 5g, h, i refer to the probability values related to Lake Ohrid for Method C (MA_agg maps).

In order to fit the problem into a linear regression framework, a 'link function' is used so that the forecast is actually the probability of tephra being observed. Here we use the logit link function, which works out as

$$P(obs) = \frac{exp(Y)}{1 + exp(Y)} \tag{4}$$

where $P$(obs) is the probability of observing a tephra, and $Y$ is the result of the linear regression. Equation (*) maps $Y \in (-\infty,\infty)$ to $P(\text{obs}) \in (0,1)$. If our models are accurate, there should be a very strong correlation between the probabilities produced from the maps and those of the logistic regression.

The best test of the models is to find that they synthesise all the useful information about the likelihood of tephra observation. However, there are a number of possible independent (predictor) variables that may provide information about the likelihood of observing a tephra including, but not necessarily limited to, the distance, the column height, the age of the tephra (a proxy for preservation), degrees off axis from the prevailing wind, whether the location corresponds to a lake or a marine core and the identity of the volcano. The first 4 factors are continuous variables, the last two categorical.

The probability maps MA_phi4 and MA_agg, relating to the source of Somma Vesuvius were mainly used. However, this methodology requires more data than those present in just the two lake sediment cores, and an extension to more eruptions, which is only possible by considering additional volcanoes. Considering this need of the model and taking into consideration the wind distribution diagrams built in relation to our study area (Fig. 4), which did not show particular differences in the various areas of the Mediterranean, we can use the same maps with a simple translation from values of the coordinates of Somma Vesuvius to those of the other three eruptive sources, Mount Etna, the Aeolian Islands and Campi Flegrei.

Specifically, to consider other volcanoes besides Somma Vesuvius, we determined the coordinate change needed to move the new considered volcano to the Somma Vesuvius position, and then we applied this coordinate transformation also to the core position, creating a new pseudo-location also for the various deposits considered. It is also important to underline that the general topography has been neglected, in fact cases are taken into consideration in which the topographic altitude of the eruptive vent is higher than the general topographic difference in level. Specifically, the Ma_phi4 and MA_agg maps relating to the source of Somma Vesuvius were also used in relation to the eruptive sources of Mount Etna, the Aeolian Islands and Campi Flegrei. In first approximation, we neglect the potential effect of topography (that is, the altitude of the potential vents), including for Mount Etna. The consideration of more eruptive sources within the model also becomes useful for taking into consideration a greater amount and range of eruption source parameters relating to the tephras found in cores positioned in a different area than the dispersion zone towards the east of Somma Vesuvius.

The additional cores considered are (Fig. 1a): KET80–04, KET80–03, KET80–11, TIR2000-C1, C1, CP10BC, UM42BC, V1069, RC9–191, TEA C-6, GT2, GT89–3, MD 90–918, AD91–17, IN68–5, CSS00–12, C0S00–7, MD 9091–7, SA03–11, SW104-ND, IN68–9, C0S01–16, AMC99–7 (Paterne et al., 1988; Di Roberto et al., 2008; Insinga et al., 2019; Di Donato et al., 2019; Crocitti et al., 2018; Castagnoli, 1990; Caron et al., 2012; Marchini et al., 2014; Calanchi and Dinelli, 2008; Siani et al., 2004; Matthews et al., 2015; Jalali et al., 2018).

The dependent variable considered in the logistic regression model is the presence or absence of tephra in the core sample, using all known eruptions from Somma Vesuvius, Campi Flegrei, Mount Etna, and the Aeolian Islands that occurred between 39 ka and 1779 CE. In order to determine whether the observation pattern is satisfactorily explained by the probability values determined by the maps at the cores' sample point, we include in the initial model other potential explanatory variables:

- Heights of the eruptive columns associated with the defined explosive eruptions;
- Distances (km) and azimuth (in degrees off-axis from the prevailing wind) between the cores and the eruptive sources;
- Age, as a proxy/test for incompleteness;
- A differential preservation effect, allowing for lakes to preserve more tephra than ocean cores;
- A volcano-specific term, as a test of homogeneity.

The goal of this logistic regression model is to is to consider the effects of the dependent variables, including the significance associated to each of these factors (Kereszturi et al., 2017), and compare the probability results of the MA_phi4 and MA_agg maps with the tephrostratigraphic data, thus determining which of the two maps/methods best models the observed dispersion of volcanic ash.

Potential model deficiencies would be indicated by significant terms involving distance, azimuth or column height, as these factors are built into the model. A significant age effect would suggest a preservation bias. Preservation has to be corrected for lake cores, which should preserve more tephra, hence the indicator for this. Finally, a significant of the volcano- specific term effect would indicate that the spatial transformation used is inappropriate.

For the case of MA_phi4 maps, stepwise regression yielded a model (significant terms only):

$$P(observed) = \frac{e^{Y}}{1+e^{Y}} \tag{5}$$

$$\text{with } Y = 1.794 I_{LAKE} - 0.00306D + 0.647 log\frac{p}{1-p} \tag{6}$$

where $I_{LAKE} = 1$ is the site is a lake, 0 if a marine core, $D$ is distance from the volcano in km, and $p$ is the forecast probability from the map model. The $P$-values for the terms were $< 0.001$ for $I_{LAKE}$. 0.009 for $p$ (i.e., the model/map) and 0.018 for $D$. This means that the probability map explains all the dependencies, with the exception of the impact on preservation that occurs for lake samples (as expected) and a residual dependency on the distance that is not fully captured by the map. The R-squared value was 15.9%, indicating a high degree of random variability expected in the process. All the other investigated features are found not significant, meaning that the model accounts for all the information contained in them. In particular, age ($P$ value $= 0.316$) is found non significant, meaning that wind distribution is representative enough also for older eruptions. The individual volcano terms had P-values between 0.581 and 0.723, meaning that the coordinate transformation is sufficient, and no further corrections (including for topography) are required. Eruptive column height, volume and azimuth were not significant too, with P-values of 0.932, 0.288 and 0.584, respectively, indicating that the map probabilities have incorporated all the useful information from them, and no missing trends exist.

Based on these results, the following conclusions can be drawn:

- The probabilities derived from the maps show a significant positive correlation with the presence of tephra in the core samples and are thus a satisfactory rendering of the dispersal pattern for our purposes.
- The age of the tephra does not appear to influence its preservation within the core samples. However, as expected, it is more likely to find volcanic tephra in lake cores than in marine cores under similar eruptive conditions.
- The model successfully considers column height and azimuth as factors influencing the presence of tephra. These variables have insignificant coefficients in the model, indicating that they play no additional role in predicting the presence of ash.
- Also regarding the data on volumes, they appear to be a variable that does not influence the prediction of the presence of ash, as they present a P-values $= 0.288$. Furthermore, during the construction of the model, only 65% of the estimates of the volume of the eruptions were retrieved from the bibliography, compared to 100% of the data relating to the heights of the columns which allowed the use of more analysable data. Therefore, data relating to eruption volumes are found to be insignificant in the model.
- In contrast, distance, although incorporated in the model in a somewhat stylized manner, has a residual effect. The coefficient is negative, indicating that tephra is slightly less likely to be observed with increasing distance than the map suggests.
- The model does not show significant differences across the eruptive sources. This suggests that the model's predictive power is consistent across different eruptive centres. It also implies that the model can be applied to other volcanic areas to predict the presence of ash.

Subsequently, the binary logistic regression model was also used to test whether the incorporation of ash aggregation via the MA_agg maps better explained the observations with the aim of incorporating the study of coarser tephras into the model. Aggregation acts through time, accelerating the fall of particles, thus it may impact the decrease-with-distance of probability, eventually correcting the residual dependence not sufficiently modelled so far.

The logistic regression model is the same type as the one described above for the MA_phi4 maps. In this case, the α value in the stepwise regression was set to 0.15 after eruptive volume (with 276 missing values) was deleted. Moreover, in this analysis, both the MA_phi4 and MA_agg maps were considered as predictors. The one selected by the stepwise procedure would be the one that provides the better fit.

The observed probabilities are calculated using the eq. (4), but with

$$Y = -0.773 + 1.584 I_{LAKE} - 0.00195D + 0.507 log\frac{p}{1-p} \tag{7}$$

where the selected map (last term) term was the MA_agg map. The P-values were 0.008 (Constant $= -0.773$), $< 0.001$ ($p$ and $I_{LAKE}$) and 0.049 (D). Therefore, there is a significant agreement of data with the map, with the exception of the impact on preservation that occurs for lake samples, which is not included in the map and therefore it is expected to remain. This model somewhat corrects the residual dependence on distance, pushing the $p$-value to more acceptable levels ($> 0.01$). Age, azimuth, column height and volcano were all not significant terms, with $p$-values larger than 0.05. The R-squared value is equal to 10.29%.

Based on these results, the following conclusions can be made:

- The MA_agg method is a better description of the ash deposition, and using it renders the residual distance effect as less significant. The introduction of a constant is due to the sea cores now having a non-zero intercept.
- Using the MA_agg maps thus appears to extract the maximum of information from the available eruption source parameters. This indicates that this model can be applied to any volcanic zone characterized by ash dispersion, and best explains the decay and deposition of volcanic particles at a given distance from the eruptive source.
- It can therefore be concluded that, through this methodology, the probability to find a tephra particle of a given size at a given distance from the source can be modelled considering only the probability values derived through Method C, without analyzing other variables.

These results show that Method C is able to correctly capture all the main features emerging from data. In particular, differently from Method B, Method C is able to correctly model the attenuation with distance, highlighting the importance of including the aggregation effect to correctly capture long-range tephra deposits. Consequently, Method C is selected as the final implementation for PROMETHEUS.

## 4. Conclusions

PROMETHEUS is a simplified model that creates maps allowing us to determine the probability of finding a specific grain size of tephra at a certain distance from the eruptive source. The model is first validated based on Holocene eruptions of Somma-Vesuvius (from eruption of the Pomici di Base to the 1944 eruption), then with previously published marine and terrestrial cores in central Mediterranean, considering as potential sources Somma Vesuvius, Mount Etna, the Aeolian Islands and Campi Flegrei. The model is easy to apply, requires only basic information about high altitude winds, and it can be spatially translated to be applied to multiple volcanic sources in a given area. The validation is made assuming as correct the heights of the eruptive columns present in the literature, the stable winds relating to the last 22 ka and the vertical fall of the volcanic particles both in the sea and in the lakes. Several configuration of the models were tested, and the validation study allowed concluding that the aggregation of the particles (MA_agg maps) dominates the distribution and deposition in space, especially in areas distant from the volcano compared to other particle sizes.

This model turns out to be very useful for new volcanological studies, allowing us to better understand, thanks also to new technologies, the different eruptive histories of volcanic springs. Importantly, "Prometheus" was designed to be playable in any location. Among the data used, topography is neglected (Scollo et al., 2008). The validation demonstrated that this has been possible also for cases with significant topography, like Mt. Etna. In any case, the cases in which the topographic elevation of the eruptive vent is higher than the general topographic difference in height can be taken into consideration. Furthermore, only the easily downloadable ERA5 data relating to the wind intensity and direction characteristics and the information relating to the tephras recognized in the proximal and distal areas with respect to the volcano are used as input.

This model can be used in sigle volcanoes to to deepen a study relating to the completeness of the eruptive catalog, similarly to what we have done in the validation study for the catalog of Somma Vesuvius from eruption of the Pomici di Base to the 1944 eruption. This model will also be useful because, through the comparison of probability maps with tephrostratigraphy of marine and terrestrial cores, it will guide the location of sampling sites for a given tephra deposit and the related type of explosive eruption. By also considering longer periods of time, it will be possible to increase and improve the completeness of the eruption catalogs and better recognize the different eruptive histories.

## Author agreement statement

We the undersigned declare that this manuscript is original, has not been published before and is not currently being considered for publication elsewhere.

We confirm that the manuscript has been read and approved by all named authors and that there are no other persons who satisfied the criteria for authorship but are not listed. We further confirm that the order of authors listed in the manuscript has been approved by all of us.

We understand that the Corresponding Author is the sole contact for the Editorial process. He/she is responsible for communicating with the other authors about progress, submissions of revisions and final approval of proofs.

## Financing

We thank the Doctorate course in Geoscience at the University of Bari Aldo-Moro.

## CRediT authorship contribution statement

**E. Billotta:** Conceptualization, Data curation, Formal analysis, Resources, Software, Supervision, Validation, Visualization, Writing – original draft, Writing – review & editing. **R. Sulpizio:** Conceptualization, Data curation, Formal analysis, Funding acquisition, Methodology, Resources, Supervision, Validation, Visualization, Writing – original draft, Writing – review & editing. **J. Selva:** Conceptualization, Data curation, Formal analysis, Funding acquisition, Methodology, Resources, Software, Supervision, Validation, Visualization, Writing – original draft, Writing – review & editing. **A. Costa:** Data curation, Formal analysis, Methodology, Resources, Software, Writing – original draft, Writing – review & editing. **M. Bebbington:** Methodology, Resources, Software, Supervision, Visualization, Writing – original draft, Writing – review & editing.

## Declaration of competing interest

The authors declare that they have no competing interests.

## Data availability

Data will be made available on request. All the data necessary to evaluate the conclusions of the document are present in the document.

## Acknowledgements

We thank The University of Bari Aldo-Moro and M. Perrini, G. Gonzales Illama and S.Massaro for having contributed to the improvement of the figures in the text.

## References

Andronico, D., Cioni, R., 2002. Contrasting styles of Mount Vesuvius activity in the period between the Avellino and Pompeii Plinian eruptions, and some implications for assessment of future hazards. Bull. Volcanol. 64 (6), 372–391. https://doi.org/10.1007/s00445-002-0215-4.

Andronico, D., Cioni, R., Marianelli, P., Sbrana, A., 1995. Interplianan activity at Somma-Vesuvius: the Avellino-Pompei period. Periodico di Mineral. 64, 79–80.

Ang, P.S., Bebbington, M.S., Lindsay, J.M., Jenkins, S.F., 2020. From eruption scenarios to probabilistic volcanic hazard analysis: an example of the Auckland Volcanic Field, New Zealand. J. Volcanol. Geotherm. Res. 397 https://doi.org/10.1016/j.jvolgeores.2020.106871.

Armienti, P., Macedonio, G., Pareschi, M.T., 1988. A numerical model for simulation of tephra transport and deposition: applications to May 18, 1980, Mount St. Helens eruption. J. Geophys. Res. 93 (B6), 6463–6476. https://doi.org/10.1029/JB093iB06p06463.

Arrighi, S., Principe, C., Rosi, M., 2001. Violent strombolian and subplinian eruptions at Vesuvius during post-1631 activity. Bull. Volcanol. 63 (2–3), 126–150. https://doi.org/10.1007/s004450100130.

Bebbington, M., 2013. Models for Temporal Volcanic Hazard. Statis. in Volcan. 1, 1–24. https://doi.org/10.5038/2163-338x.1.1.

Bebbington, M.S., 2020. Temporal-volume probabilistic hazard model for a supervolcano: Taupo, New Zealand. Earth and Planetary Science letters, 536, 116141.Brown, R. J., Bonadonna, C., & Durant, A. J. (2012). A review of volcanic ash aggregation. Phys. Chem. Earth 45–46, 65–78. https://doi.org/10.1016/j.pce.2011.11.001.

Bebbington, M.S., Lai, C.D., 1998. A generalized negative binomial and applications. Commun. in Statis. - Theory and Meth. 27 (10), 2515–2533. https://doi.org/10.1080/03610929808832240.

Bertagnini, A., Landi, P., Rosi, M., Vigliargio, A., 1998. The Pomici di Base plinian eruption of Somma-Vesuvius. J. Volcanol. Geotherm. Res. 83 (3–4), 219–239.

Brown, R.J., Bonadonna, C., Durant, A.J., 2012. A review of volcanic ash aggregation. Physics and Chemistry of the Earth, Parts a/b/c 45, 65–78.

Calanchi, N., Dinelli, E., 2008. Tephrostratigraphy of the last 170 ka in sedimentary successions from the Adriatic Sea. J. Volcanol. Geotherm. Res. 177 (1), 81–95. https://doi.org/10.1016/j.jvolgeores.2008.06.008.

Caron, B., Siani, G., Sulpizio, R., Zanchetta, G., Paterne, M., Santacroce, R., Tema, E., Zanella, E., 2012. Late Pleistocene to Holocene tephrostratigraphic record from the

Northern Ionian Sea. Mar. Geol. 311–314, 41–51. https://doi.org/10.1016/j.margeo.2012.04.001.
Castagnoli C., Bonino, G., G., Callegari, E., Guang-Mei Zhu (1990). Radiometric and Tephroanalysis Dating of Recent Ionian Sea Cores.
Cioni, R., Gurioli, L., Sbrana, A., Vougioukalakis, G., 2000. Precursory Phenomena And Destructive Events Related to the Late Bronze Age Minoan (Thera, Greece) and AD 79 (Vesuvius, Italy) Plinian Eruptions; Inferences From The Stratigraphy in the Archaeological Areas The Minoan Eruption. http://sp.lyellcollection.org/.
Cioni, R., Gurioli, L., Lanza, R., Zanella, E., 2004. Temperatures of the a.D. 79 pyroclastic density current deposits (Vesuvius, Italy). J. Geophys. Res. Solid Earth 109 (B2). https://doi.org/10.1029/2002jb002251.
Cioni, R., Bertagnini, A., Santacroce, R., Andronico, D., 2008. Explosive activity and eruption scenarios at Somma-Vesuvius (Italy): Towards a new classification scheme. J. Volcanol. Geotherm. Res. 178 (3), 331–346. https://doi.org/10.1016/j.jvolgeores.2008.04.024.
Cole, P.D., Scarpati, C., 2010. The 1944 eruption of Vesuvius, Italy: Combining contemporary accounts and field studies for a new volcanological reconstruction. Geol. Mag. 147 (3), 391–415. https://doi.org/10.1017/S0016756809990495.
Cornell, W., Carey, S., Sigurdsson, H., 1983. Explosive Volcanism. In. J. Volcanol. Geotherm. Res. 17.
Costa, A., 2013. Hazmap. https://theghub.org/resources/hazmap.
Costa, A., Macedonio, G., Folch, A., 2006. A three-dimensional Eulerian model for transport and deposition of volcanic ashes. Earth Planet. Sci. Lett. 241 (3–4), 634–647. https://doi.org/10.1016/j.epsl.2005.11.019.
Costa, A., Folch, A., Macedonio, G., 2010. A model for wet aggregation of ash particles in volcanic plumes and clouds: 1. Theoretical formulation. J. Geophys. Res. Solid Earth 115 (B9).
Costa, A., Pioli, L., Bonadonna, C., 2016. Assessing tephra total grain-size distribution: Insights from field data analysis. Earth Planet. Sci. Lett. 443, 90–107. https://doi.org/10.1016/j.epsl.2016.02.040.
Cottrell, E., Siebert, L., Kimberly, P., 2010, December. The Future of Smithsonian's Global Volcanism Program. In: AGU Fall Meeting Abstracts, Vol. 2010, p. V43E-04.
Crocitti, M., Sulpizio, R., Insinga, D.D., De Rosa, R., Donato, P., Iorio, M., Zanchetta, G., Barca, D., Lubritto, C., 2018. On ash dispersal from moderately explosive volcanic eruptions: examples from Holocene and late Pleistocene eruptions of Italian volcanoes. J. Volcanol. Geotherm. Res. 385, 198–221. https://doi.org/10.1016/j.jvolgeores.2018.07.009.
Crosweller, H.S., Arora, B., Brown, S.K., Cottrell, E., Deligne, N.I., Guerrero, N.O., Hobbs, L., Kiyosugi, K., Loughlin, S.C., Lowndes, J., Nayembil, M., Siebert, L., Sparks, R.S.J., Takarada, S., Venzke, E., 2012. Global database on large magnitude explosive volcanic eruptions (LaMEVE). J. Appl. Volcanol. 1 (1) https://doi.org/10.1186/2191-5040-1-4.
Davis, J.C., Wiley, J., New York Clxchester Brisbane Toronto Singapore, S, 2002. Statistics and Data Analysis Third Edition.
Dellino, P., Mele, D., Bonasia, R., Braia, G., La Volpe, L., Sulpizio, R., 2005. The analysis of the influence of pumice shape on its terminal velocity. Geophys. Res. Lett. 32 (21), 1–4. https://doi.org/10.1029/2005GL023954.
Di Donato, V., Insinga, D.D., Iorio, M., Molisso, F., Rumolo, P., Cardines, C., Passaro, S., 2019. The palaeoclimatic and palaeoceanographic history of the Gulf of Taranto (Mediterranean Sea) in the last 15 ky. Glob. Planet. Chang. 172, 278–297. https://doi.org/10.1016/j.gloplacha.2018.10.014.
Di Roberto, A., Rosi, M., Bertagnini, A., Marani, M.P., Gamberi, F., Del Principe, A., 2008. Deep water gravity core from the Marsili Basin (Tyrrhenian Sea) records Pleistocenic-Holocenic explosive events and instability of the Aeolian Archipelago, (Italy). J. Volcanol. Geotherm. Res. 177 (1), 133–144. https://doi.org/10.1016/j.jvolgeores.2008.01.009.
Folch, A., 2012. A review of tephra transport and dispersal models: Evolution, current status, and future perspectives. In J. Volcanol. Geotherm. Res. 235–236, 96–115. https://doi.org/10.1016/j.jvolgeores.2012.05.020.
Folch, A., Costa, A., Durant, A., Macedonio, G., 2010. A model for wet aggregation of ash particles in volcanic plumes and clouds: 2. Model application. J. Geophys. Res. Solid Earth 115 (B9).
Francke, A., Dosseto, A., Panagiotopoulos, K., Leicher, N., Lacey, J.H., Kyrikou, S., Wagner, B., Zanchetta, G., Kouli, K., Leng, M.J., 2019. Sediment residence time reveals Holocene shift from climatic to vegetation control on catchment erosion in the Balkans. Glob. Planet. Chang. 177, 186–200. https://doi.org/10.1016/j.gloplacha.2019.04.005.
Grezio, A., Lorito, S., Parsons, T., Selva, J., 2017. Tsunamis: Bayesian Probabilistic Analysis. In: Encyclopedia of Complexity and Systems Science. Springer, Berlin Heidelberg, pp. 1–25. https://doi.org/10.1007/978-3-642-27737-5_645-1.
Insinga, D.D., Petrosino, P., Alberico, I., de Lange, G.J., Lubritto, C., Molisso, F., Sacchi, M., Sulpizio, R., Wu, J., Lirer, F., 2019. The late Holocene tephra record of the Central Mediterranean Sea: Mapping occurrences and new potential isochrons for the 4.4–2.0 ka time interval. J. Quat. Sci. 35 (1–2), 213–231. https://doi.org/10.1002/jqs.3154.
Jalali, B., Sicre, M.A., Klein, V., Schmidt, S., Maselli, V., Lirer, F., Bassetti, M.A., Toucanne, S., Jorry, S.J., Insinga, D.D., Petrosino, P., Châles, F., 2018. Deltaic and Coastal Sediments as Recorders of Mediterranean Regional climate and Human Impact over the past three Millennia. Paleocean. and Paleoclim. 33 (6), 579–593. https://doi.org/10.1029/2017PA003298.
Keller, J., Ryan, W.B.F., Ninkovich, D., Altherr, R., 1978. Explosive volcanic activity in the Mediterranean over the past 200,000 yr as recorded in deep-sea sediments. Geol. Soc. Am. Bull. 89 (4), 591–604.
Kereszturi, G., Bebbington, M., Németh, K., 2017. Forecasting transitions in monogenetic eruptions using the geologic record. Geology 45 (3), 283–286. https://doi.org/10.1130/G38596.1.
Lautenschlager, Michael, Herterich, Klaus, 1990. Atmospheric response to ice age conditions: Climatology near the Earth's surface. J. Geophys. Res. Atmos. 95 (D13), 22547–22557.
Leicher, N., Zanchetta, G., Sulpizio, R., Giaccio, B., Wagner, B., Nomade, S., Francke, A., Del Carlo, P., 2016. First tephrostratigraphic results of the DEEP site record from Lake Ohrid (Macedonia and Albania). Biogeosciences 13 (7), 2151–2178. https://doi.org/10.5194/bg-13-2151-2016.
Leicher, N., Giaccio, B., Zanchetta, G., Wagner, B., Francke, A., Palladino, D.M., Sulpizio, R., Albert, P.G., Tomlinson, E.L., 2021. Central Mediterranean explosive volcanism and tephrochronology during the last 630 ka based on the sediment record from Lake Ohrid. Quat. Sci. Rev. 226 https://doi.org/10.1016/j.quascirev.2019.106021.
Lowe, D.J., 2011. Tephrochronology and its application: A review. In: Quaternary Geochronology, Vol. 6, Issue 2, pp. 107–153. https://doi.org/10.1016/j.quageo.2010.08.003.
Macedonio, G., Costa, A., Longo, A., 2005. A computer model for volcanic ash fallout and assessment of subsequent hazard. Comput. Geosci. 31 (7), 837–845. https://doi.org/10.1016/j.cageo.2005.01.013.
Marchini, G., Zanchetta, G., Santacroce, R., Vigliotti, L., Capotondi, L., Sulpizio, R., 2014. Tephrostratigraphy of marine CORE AD91-17 (Adriatic Sea) revised Paleolithic and Mesolithic of Southern Italy and Sicily View project FUTURE: FUcino Tephrochronology Unites Quaternary REcords View project TEPHROSTRATIGRAPHY OF MARINE CORE AD91-17 (ADRIATIC SEA) REVISED, Vol. 27, issue 2. https://www.researchgate.net/publication/270567946.
Martínez-Martínez, J., Abellán, A., Berrezueta, E., 2022. Erosion directionality and seasonality study using the anisotropy matrix. Application in a semiarid Mediterranean climate (SE Spain). Sci. Total Environ. 804, 150165.
Massaro, S., Stocchi, M., Martínez Montesinos, B., Sandri, L., Selva, J., Sulpizio, R., Costa, A., 2023. Assessing long-term tephra fallout hazard in southern Italy from Neapolitan volcanoes. Nat. Hazards Earth Syst. Sci. 23 (6), 2289–2311.
Matthews, I.P., Trincardi, F., Lowe, J.J., Bourne, A.J., MacLeod, A., Abbott, P.M., Andersen, N., Asioli, A., Blockley, S.P.E., Lane, C.S., Oh, Y.A., Satow, C.S., Staff, R. A, Wulf, S., 2015. Developing a robust tephrochronological framework for late Quaternary marine records in the Southern Adriatic Sea: New data from core station SA03-11. Quat. Sci. Rev. 118, 84–104. https://doi.org/10.1016/j.quaint.2011.07.010.
Mead, S., Magill, C., 2014. Determining change points in data completeness for the Holocene eruption record. Bull. Volcanol. 76, 1–14.
Mele, D., Sulpizio, R., Dellino, P., la Volpe, L., 2011. Stratigraphy and eruptive dynamics of a pulsating Plinian eruption of Somma-Vesuvius: the Pomici di Mercato (8900 years B.P.). Bull. Volcanol. 73 (3), 257–278. https://doi.org/10.1007/s00445-010-0407-2.
Narcisi, B., 1996. Tephrochronology of a late Quaternary Lacustrine record: from the Monticchio Maar (Vulture Volcano, Southern Italy). In Quat. Sci. Rev. 15.
Paterne, M., Guichard, F., Labeyrie, J., 1988. Explosive activity of the South Italian Volcanoes during the past 80,000 years as determined by marine tephrochronology. In J. Volcanol. Geotherm. Res. 34.
Pfeiffer, T., Costa, A., Macedonio, G., 2005. A model for the numerical simulation of tephra fall deposits. J. Volcanol. Geotherm. Res. 140 (4), 273–294. https://doi.org/10.1016/j.jvolgeores.2004.09.001.
Rose, W.I., Durant, A.J., 2009. Fine ash content of explosive eruptions. J. Volcanol. Geotherm. Res. 186 (1–2), 32–39.
Rosi, M., Santacroce, R., 1983. Explosive Volcanism. In J. Volcanol. Geotherm. Res. 17.
Sandri, L., Costa, A., Selva, J., Tonini, R., Macedonio, G., Folch, A., Sulpizio, R., 2016. Beyond eruptive scenarios: assessing tephra fallout hazard from Neapolitan volcanoes. Sci. Rep. 6 (1), 24271.
Santacroce, R., 1987. Volcanic Hazard Assessment in the Phlegraean Fields: A Contribution Based on Stratigraphic and Historical Data.
Santacroce, R., Cioni, R., Marianelli, P., Sbrana, A., Sulpizio, R., Zanchetta, G., Donahue, D.J., Joron, J.L., 2008. Age and whole rock-glass compositions of proximal pyroclastics from the major explosive eruptions of Somma-Vesuvius: a review as a tool for distal tephrostratigraphy. J. Volcanol. Geotherm. Res. 177 (1), 1–18. https://doi.org/10.1016/j.jvolgeores.2008.06.009.
Scollo, S., Folch, A., Costa, A., 2008. A parametric and comparative study of different tephra fallout models. J. Volcanol. Geotherm. Res. 162, 199–211. https://doi.org/10.1016/j.jvolgeores.2008.04.00.
Selva, J., 2013. Long-term multi-risk assessment: Statistical treatment of interaction among risks. Nat. Hazards 67 (2), 701–722. https://doi.org/10.1007/s11069-013-0599-9.
Siani, G., Sulpizio, R., Paterne, M., Sbrana, A., 2004. Tephrostratigraphy study for the last 18,000 14C years in a deep-sea sediment sequence for the South Adriatic. Quat. Sci. Rev. 23 (23–24), 2485–2500. https://doi.org/10.1016/j.quascirev.2004.06.004.
Sigurdsson, Haraldur, Cashdollar, Stanford, Sparks, Stephen R.J., 1982. The eruption of Vesuvius in AD 79: reconstruction from historical and volcanological evidence. Am. J. Archaeol. 86 (1), 39–51.
Sparks, R.S.J., Aspinall, W.P., 2004. Volcanic activity: Frontiers and challenges in forecasting, prediction and risk assessment. In: Geophysical Monograph Series, vol. 150. Blackwell Publishing Ltd., pp. 359–373. https://doi.org/10.1029/150GM28
Sulpizio, R., Mele, D., Dellino, P., La Volpe, L., 2005. A complex, Subplinian-type eruption from low-viscosity, phonolitic to tephri-phonolitic magma: the AD 472 (Pollena) eruption of Somma-Vesuvius, Italy. Bull. Volcanol. 67 (8), 743–767. https://doi.org/10.1007/s00445-005-0414-x.
Sulpizio, R., De Rosa, R., Donato, P., 2008. The influence of variable topography on the depositional behaviour of pyroclastic density currents: the examples of the Upper Pollara eruption (Salina Island, southern Italy). J. Volcanol. Geotherm. Res. 175 (3), 367–385. https://doi.org/10.1016/j.jvolgeores.2008.03.018.

Sulpizio, R., Van Welden, A., Caron, B., Zanchetta, G., 2010. The Holocene tephrostratigraphic record of Lake Shkodra (Albania and Montenegro). J. Quat. Sci. 25 (5), 633–650. https://doi.org/10.1002/jqs.1334.

Sulpizio, R., Zanchetta, G., Vogel, H., Wagner, B., 2014. Tephra layers in lakes Ohrid and Prespa Tephrostratigraphy and tephrochronology of lakes Ohrid and Prespa. Balkans Tephra layers in lakes Ohrid and Prespa. https://doi.org/10.5194/bgd-7-3931-2010.

Vecino, M.C.D., Rossi, E., Freret-Lorgeril, V., Fries, A., Gabellini, P., Lemus, J., Pollastri, S., Poulidis, A.P., Iguchi, M., Bonadonna, C., 2022. Aerodynamic characteristics and genesis of aggregates at Sakurajima Volcano, Japan. Sci. Rep. 12 (1) https://doi.org/10.1038/s41598-022-05854-z.

Vogel, H., Zanchetta, G., Sulpizio, R., Wagner, B., Nowaczyk, N., 2010. A tephrostratigraphic record for the last glacial-interglacial cycle from Lake Ohrid, Albania and Macedonia. J. Quat. Sci. 25 (3), 320–338. https://doi.org/10.1002/jqs.1311.

Wagner, B., Sulpizio, R., Zanchetta, G., Wulf, S., Wessels, M., Daut, G., Nowaczyk, N., 2008. The last 40 ka tephrostratigraphic record of Lake Ohrid, Albania and Macedonia: a very distal archive for ash dispersal from Italian volcanoes. J. Volcanol. Geotherm. Res. 177 (1), 71–80. https://doi.org/10.1016/j.jvolgeores.2007.08.018.

Wagner, B., Vogel, H., Francke, A., Friedrich, T., Donders, T., Lacey, J.H., Leng, M.J., Regattieri, E., Sadori, L., Wilke, T., Zanchetta, G., Albrecht, C., Bertini, A., Combourieu-Nebout, N., Cvetkoska, A., Giaccio, B., Grazhdani, A., Hauffe, T., Holtvoeth, J., Zhang, X., 2019. Mediterranean winter rainfall in phase with African monsoons during the past 1.36 million years. Nature 573 (7773), 256–260. https://doi.org/10.1038/s41586-019-1529-0.

Wang, T., Schofield, M., Bebbington, M., Kiyosugi, K., 2020. Bayesian modelling of marked point processes with incomplete records: volcanic eruptions. J. R. Stat. Soc.: Ser. C: Appl. Stat. 69 (1), 109–130.

Wulf, S., Kraml, M., Brauer, A., Keller, J., Negendank, J.F.W., 2004. Tephrochronology of the 100ka lacustrine sediment record of Lago Grande di Monticchio (southern Italy). Quat. Int. 122 (1 SPEC. ISS), 7–30. https://doi.org/10.1016/j.quaint.2004.01.028.

Wulf, S., Kraml, M., Keller, J., 2008. Towards a detailed distal tephrostratigraphy in the Central Mediterranean: the last 20,000 yrs record of Lago Grande di Monticchio. J. Volcanol. Geotherm. Res. 177 (1), 118–132. https://doi.org/10.1016/j.jvolgeores.2007.10.009.

Wulf, S., Keller, J., Paterne, M., Mingram, J., Lauterbach, S., Opitz, S., Sottili, G., Giaccio, B., Albert, P.G., Satow, C., Tomlinson, E.L., Viccaro, M., Brauer, A., 2012. The 100-133 ka record of Italian explosive volcanism and revised tephrochronology of Lago Grande di Monticchio. Quat. Sci. Rev. 58, 104–123. https://doi.org/10.1016/j.quascirev.2012.10.020.